BUTTERWORTH HEINEMANN

Concentric annular flow with centerbody rotation of a Newtonian and a shear-thinning liquid

M. P. Escudier and I. W. Gouldson
University of Liverpool, Department of Mechanical Engineering, Liverpool, UK

Measurements of the radial distributions of the axial and tangential components of velocity and rms velocity fluctuations are presented together with friction factor *versus* Reynolds number data for two liquids, one Newtonian, the other a shear-thinning polymer, in laminar, transitional, and turbulent flow in an annular geometry with a rotating centerbody of radius ratio 0.506. In all flow regimes, the friction factor is increased by centerbody rotation. However, the influence is slight and most apparent for laminar flow of the Newtonian fluid. Laser Doppler anenometry (LDA) measurements of the tangential velocity reveal three distinct regions across the radial gap with a central region of almost constant angular momentum, which diminishes in magnitude as the Reynolds number increases. Axial velocity measurements show only slight deviations from what would be expected for the case without centerbody rotation. In turbulent flow, the axial velocity fluctuations decrease progressively with increasing Reynolds number for all fluids. For the polymeric liquid, the tangential velocity fluctuations are somewhat suppressed, especially at high Reynolds numbers where the influence of centerbody rotation is reduced. Over a limited range of (low) Reynolds numbers and rotation speeds, the generation and advection of Taylor vortices produces complex flow patterns. Limited measurements are reported for the vortex advection speed.

Keywords: concentric annulus; centerbody rotation; shear-thinning; non-Newtonian

Introduction

Cuttings transport, diffusion and advection of dissolved gas, gas bubble rise, and the build-up of mud cake on the borehole wall are all directly affected by the flow of drilling fluid ("mud"), which is pumped up the annulus created between the rotating drill pipe and the bore hole wall during the drilling of oil and gas wells. The flow is further complicated by the fact that most drilling muds are shear thinning, viscoelastic, and thixotropic (Alderman et al. 1988), that the drill pipe is invariably offset (eccentric) to an unknown extent, and that the bore hole geometry is not precisely defined. The work reported here is part of a program of research aimed at improving the level of understanding of well bore fluid mechanics primarily through idealized laboratory experiments. The shear-thinning liquid was selected because it has rheological characteristics similar, in part, to those of a typical drilling fluid but is optically transparent, thereby allowing the use of LDA for the measurement of flow velocities and turbulence intensities. The experimental flow geometry is that of a concentric smooth walled annulus with a rotating centerbody of radius ratio 0.506, which is representative of a typical drill pipe/well bore. The results of experiments for this geometry without centerbody rotation have been reported recently by Escudier et al. (1995a) and for rotation without an axial flow by Escudier et al. (1995b).

Previous experimental work directly comparable to that discussed here is limited to the recent paper of Nouri and Whitelaw (1994) concerned with the flow of 0.2% aqueous carboxymethylcellulose (CMC) in an annulus with $R_i = 20$ mm and radius ratio 0.5. The only other detailed investigations involving non-Newtonian fluids are those of Nouar et al. (1987) and Naimi et al. (1990), both on the same apparatus for which the radius ratio was 0.62. The former used a highly concentrated (3%) solution of CMC in water and the latter a 0.2% aqueous solution of Carbopol. The CMC solution used in the present work is a shear-thinning polymer that is neither thixotropic nor significantly elastic at the concentration used here, 0.2% w/w. The foregoing also applies to Carbopol which, however, differs from the other fluids in exhibiting a measurable yield stress. Measurements are also reported here for a Newtonian fluid (50% w/w water/glucose solution) for which previous data are again very limited: apart from Nouri and Whitelaw's (1994) data for a mixture of tetraline and turpentine, the only other detailed data for a Newtonian fluid

Address reprint requests to M. P. Escudier, Department of Mechanical Engineering, The University of Liverpool, Liverpool L69 3BX, UK.

Received 13 October 1994; accepted 8 February 1995

Int. J. Heat and Fluid Flow 16: 156–162, 1995

655 Avenue of the Americas, New York, NY 10010

0142-727X/95/$10.00
SSDI 0142-727X(95)00012-F

are those for airflow reported by Kuzay and Scott (1973) for a radius ratio of 0.56 and by Simmers and Coney (1979) for a narrow annulus of radius ratio 0.955. Some aspects of previous work on the distribution of velocity in an annulus for high Taylor numbers in the absence of an axial flow are also relevant, particularly that of Taylor (1935). Other related experimental work has been concerned primarily with the problem of instability of helical flow and with the occurrence of Taylor vortices and their subsequent behavior in the presence of a bulk axial flow. Although, for the most part, this previous work has been limited to flow of a Newtonian fluid, an exception is the work of Wroński and Jastrzębski (1990a, b) for which relatively high concentrations (0.45–0.8%) of CMC and 1% methylcellulose were used. These investigators concluded that their results could be correlated using the usual dimensionless parameters calculated on the basis of a theoretical viscosity spatially averaged across the annular gap for unidirectional laminar flow of a power-law fluid. This procedure is evidently of limited value for flows that depart significantly from being laminar and unidirectional and for fluids that are not well described by the power-law model.

There is a considerable body of theoretical and computational work almost exclusively concerned with laminar flow. Recent work includes that of Bittleston and Hassager (1992) and of Malik and Shenoy (1991), concerned with generalized annular Couette flow of shear-thinning liquids. Of more direct relevance to the present work is the paper of Lockett et al. (1992), concerned with the stability of inelastic non-Newtonian liquids in Couette flow, as well as the extensive study of Lockett (1992), which considers the more general situation of combined axial and rotational motion. The turbulent flow problem for a Newtonian fluid was treated by Sharma et al. (1976) who gave detailed consideration to the data of Kuzay and Scott (1973).

Experimental rig and instrumentation

The flow loop used for the experiments is shown schematically in Figure 1. Flow is provided by a progressive cavity pump [1]* (Mono type E101, maximum flow rate 0.025 m^3/s) fed directly from a 500 l capacity stainless steel tank [2]. Three accumulators [3] located immediately after the Mono pump outlet act to remove pulsations in the flow prior to entry into the test geometry [4]. The annular test section consists of six precision-bore borosilicate glass tubes, (i.d. 100.4 ± 0.1 mm) with a 50.8-mm diameter stainless steel inner tube [5], giving a radius ratio of 0.506. The outer pipe glass tubes are assembled into modules with matched male/female stainless steel flanges at alternate ends. Each glass tube is separated from the stainless steel by a PTFE ring, and each end of a module (assembled in a jig) is fixed using Devcon urethane rubber. The test section consists of five modules each of 1.027 m length and one of 0.64 m, which gives an overall length of 5.775 m and a length-to-hydraulic diameter ratio of 116. To minimize sagging of the inner tube, the centerbody wall thickness was selected to provide near-neutral buoyancy in the water-based test fluids. In addition, a three ton axial load is applied by means of a hydraulic jack [6]. The centerbody may be rotated at any speed up to a maximum of 126 rpm by means of a DC Neco motor and gearbox [7]. Centerbody speed measurements were made by means of a slotted disk and optical encoder arrangement [8] giving a resolution of 0.1 rpm. In practice, the centerbody is slightly distorted, and it has proved impossible to achieve a concentric geometry over the entire length of the test section. Detailed measurements were made at a location 600 mm (245 gap widths) from the downstream endhousing. Considerable effort was directed at minimizing departures from concentricity, particularly at this location where the maximum deviation was determined to be less than 3% in both the horizontal and vertical planes.

Pressure tappings of 1 mm diameter are provided on each mating flange pair with 3 mm internal diameter clear vinyl tubing [9], filled with deionized water, connecting each pressure tapping via a series of valves [10] to two Validyne differential pressure transducers [11] (DP15-26, 3448 Pa fsd and DP15-20 862 Pa fsd). The valves are connected to the pipe tappings in such a way as to permit measurement of the pressure drop over increasing numbers of pipe sections to assess the location at which fully developed flow is achieved. Signal conditioning for the pressure transducers is provided by a Validyne CD223 digital transducer indicator with a BCD output to a data-logging computer (IBM AT 286 PC). The transducers were calibrated in air at periodic intervals against a Baratron 398HD-01000SP05 (1000 Torr fsd) high-precision differential pressure transducer with an accuracy over the calibration range of 0.01% of reading. The accuracy of the Validyne transducers is estimated to be better than $\pm 1\%$ of reading. A platinum resistance thermometer [12] mounted in the endhousing downstream of the test section is used to monitor the fluid temperature to an accuracy of $\pm 0.1°C$.

The mean velocity and turbulence intensities were determined using a Dantec Fibreflow LDA system comprising of a 60X10 probe and 55X12 beam expander [13] together

* The numbers in brackets refer to the components shown in Figure 1.

Notation

C	constant in $wr = C\omega R_i^2$
f	friction factor $2\tau_s/\rho U^2$
L	axial length, m
n	power-law exponent
$\dot{Q}$	volumetric flow rate, m^3/s
r	radial location in annulus, m
Re	bulk flow Reynolds number $2\rho U(R_o - R_i)/\mu$
R_i	outer radius of centerbody, m
R_o	inner radius of outer wall of annulus, m
Ta	Taylor number $(\rho\omega/\mu)^2 R_i(R_o - R_i)^3$
u	mean axial velocity component, m/s
u'	rms value of fluctuating axial velocity, m/s
u_C	value of u' at $\xi = 0.8$, m/s
U	bulk axial velocity $\dot{Q}/\pi(R_o^2 - R_i^2)$, m/s
w	mean tangential velocity component, m/s
w'	rms value of fluctuating tangential velocity component, m/s

Greek

Δp	pressure drop over length L, Pa
$\dot{\gamma}$	shear rate, 1/s
λ_C	constant in Cross model, s
λ_n	constant in power-law model, s
μ	characteristic fluid viscosity, Pa·s
μ_0	zero shear-rate viscosity
μ_∞	infinite shear-rate viscosity, Pa·s
ξ	nondimensional radial location $(R_o - r)/(R_o - R_i)$
ρ	fluid density, kg/m^3
τ_s	average surface shear stress, Pa
ω	centerbody rotation speed, rad/s

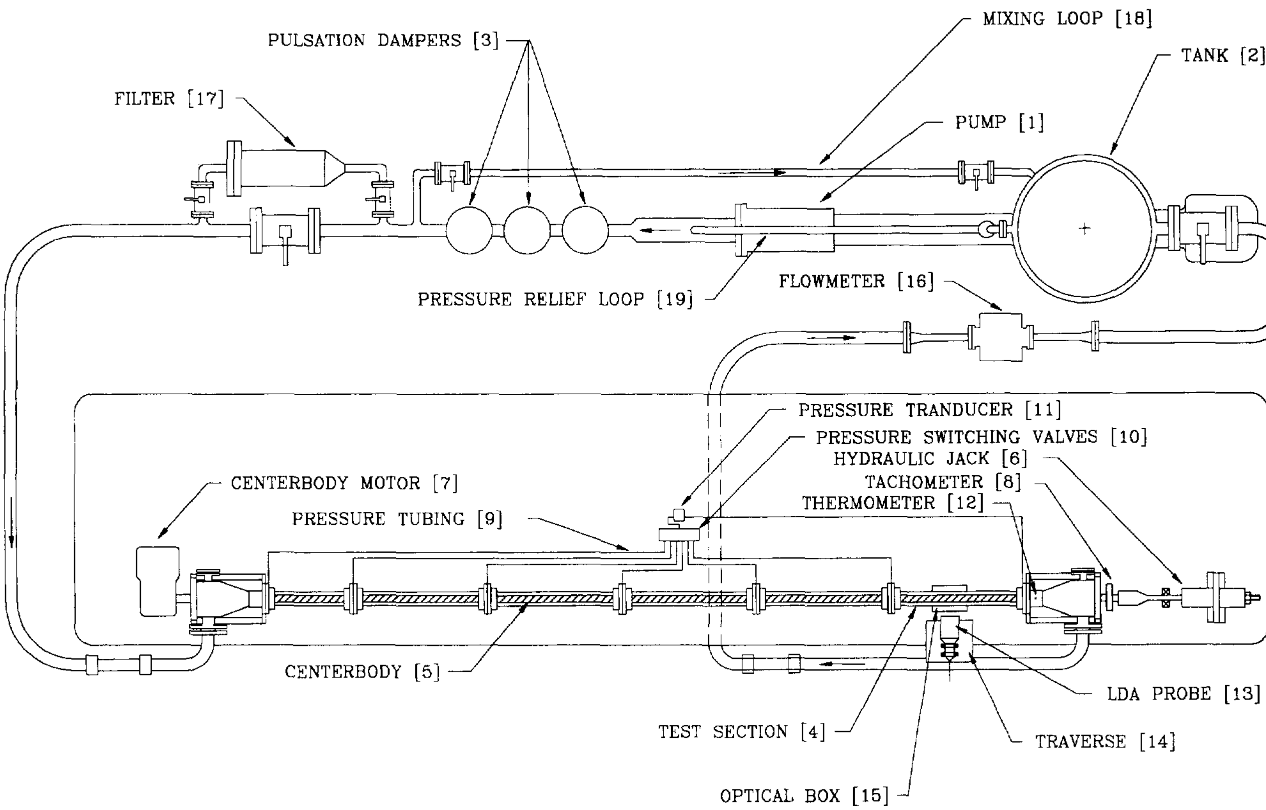

Figure 1 Plan view schematic diagram of flow loop

with a Dantec BSA 57N10 burst spectrum analyzer signal processor and a Hewlett Packard 286/12 microcomputer. The LDA optical parameters are as follows: beam separation at front lens 51.5 mm, lens focal length 160 mm, and length of principal axis of measurement volume 0.19 mm. In view of the small size of the measurement volume, it was not regarded as necessary to make a gradient correction to the measured velocities. The probe head, housing both the transmitting and receiving optics, was mounted on a three-axis traverse [14] controlled by a microcomputer (IBM XT PS2 model 30) and having a spatial resolution of 15 μm. Measurements of the axial and tangential velocities, and the corresponding turbulence intensities, were made by traversing the measuring volume radially toward the centerbody from the outer glass tube. For a few measurements, a second LDA system was employed to permit cross-correlation measurements of the velocities at two locations separated axially by either 10 mm or 20 mm and azimuthally by 90°, the azimuthal separation necessitated by the physical size of the probe heads. A flat-faced optical box [15] filled with castor oil, which had a refractive index close to that of the glass ($R_n = 1.478$), was positioned over the pipe at the measurement location to minimize refraction of the beams and, hence, simplify refraction correction calculations.

A Fischer and Porter electromagnetic flow meter [16] (model 10 D1) is incorporated in the return arm of the flow loop, with the output signal recorded via an Amplicon PS 30AT A/D converter on an IBM AT 286 PC. Flow rates indicated by the flow meter were found to be within 1% of values computed from velocity profiles measured in pipe flow using the LDA system. In-house software was written to record flow rate, pressure drop, and fluid temperature, and to control and record probe location.

To permit filtering of the base solvent (tap water) prior to the addition of polymer, a 125-μm filter [17] is incorporated into a bypass loop through which the flow can be diverted. Mixing of the polymer is accomplished by circulating the fluid through a return loop [18] to the tank incorporated just after the pulsation dampers. A pressure relief (safety) valve and return loop [19] are located immediately after the pump outlet.

The viscometric characteristics of the test fluid in use were determined using a CarriMed controlled-stress rheometer (CSL 100) with either a cone-and-plate or a parallel-plate geometry. The rheometer was controlled from a CAF 386SX PC employing CarriMed's flow equilibrium software. Fluid refractive indices were determined using an ABBE 60/ED high-accuracy refractometer.

Test fluids: preparation and rheology

For control purposes, one set of data was acquired for a Newtonian fluid: a 1:1 w/w mixture of a glucose syrup (cerestar) and water with a dynamic viscosity $\mu = 0.01$ Pa·s at 20°C. The polymer used was a high-viscosity grade of carboxymethylcellulose, sodium salt obtained for the present work from Aldrich Chemical Company, Inc. About 700 l of each fluid was prepared by filtering tap water prior to the addition of 0.2% w/w of the polymer or 50% w/w of glucose. To prevent bacteriological degradation of the fluid a small quantity of formaldehyde was added (100 ppm for CMC; 200 ppm for glucose/water). Seeding particles (Timiron MP-1005, mean diameter approximately 20 μm) at a concentration of 1 ppm were added to improve the LDA signal-to-noise ratio and data rate.

Although the viscosity data for the polymer, shown in Figure 2, are conveniently represented (for $\dot{\gamma} > 200\ \mathrm{s}^{-1}$) by $\mu = (\lambda_n \dot{\gamma})^{n-1}$ with $\lambda_n = 0.239$ s and $n = 0.69$ (curve 1), a better representation over the entire range of shear rates is given by

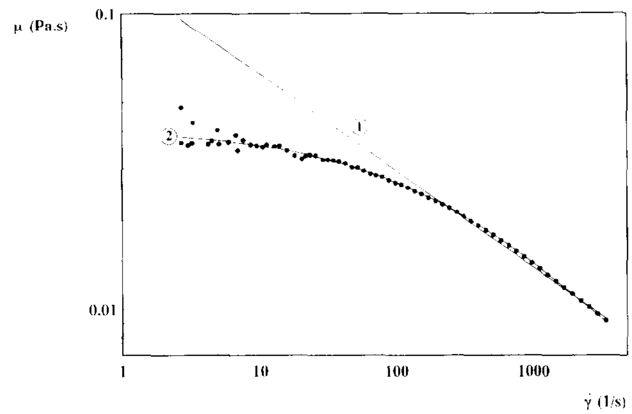

Figure 2 Viscosity *versus* shear rate for 0.2% w/w CMC; 1 power-law fit, 2 Cross model fit

the Cross model:

$$\frac{\mu - \mu_\infty}{\mu_0 - \mu_\infty} = [1 + (\lambda_C \dot{\gamma})^n]^{-1}$$

with $\mu_0 = 0.0408$ Pa · s, $\mu_\infty = 0.001$ Pa · s, $\lambda_C = 0.00329$ s, and $n = 0.563$ (curve 2).

For the evaluation of Reynolds and Taylor numbers for the CMC flows, shear rates for the determination of a characteristic fluid viscosity μ were obtained from the viscometric data using an average surface shear stress τ_s determined from the axial pressure gradient $\Delta p/L$; i.e., $\tau_s = \Delta p(R_0 - R_i)/2L$. It is recognized that this practice underestimates the shear rate, because it does not account for the contribution caused by tangential motion. As will be seen, the tangential velocity gradient close to the outer wall of the annulus is relatively well defined so that, in principle, a reliable net shear rate could be calculated. However, in the vicinity of the centerbody, the shear rate is very much higher because of the quadratic influence of R_0/R_i (this point is discussed further in the following section), and a reliable estimate is not possible.

Results

The global influence of centerbody rotation for each of the test fluids is apparent from the friction factor *versus* Reynolds number data shown in Figure 3 and the normalized axial velocity fluctuations close to the centerbody ($\xi = 0.8$) shown in Figure 4, which are used to monitor the change from laminar flow through transition to turbulent flow. For comparison purposes, curves representing standard friction-factor correlations for fully developed flow of a Newtonian fluid in an annulus with radius ratio 0.5 and no centerbody rotation are included in Figure 3 as follows:

Laminar:

$$f = 23.9/\mathrm{Re}$$

Turbulent (Jones and Leung 1981)

$$\frac{1}{\sqrt{f}} = 4 \log_{10}(1.343\ \mathrm{Re}\sqrt{f}) - 1.6$$

Also shown is a curve representing the ultimate drag reduction asymptote for this geometry suggested by Escudier et al. (1994a):

$$\frac{1}{\sqrt{f}} = 8.27 \ln(\mathrm{Re}\sqrt{f}) - 34.6$$

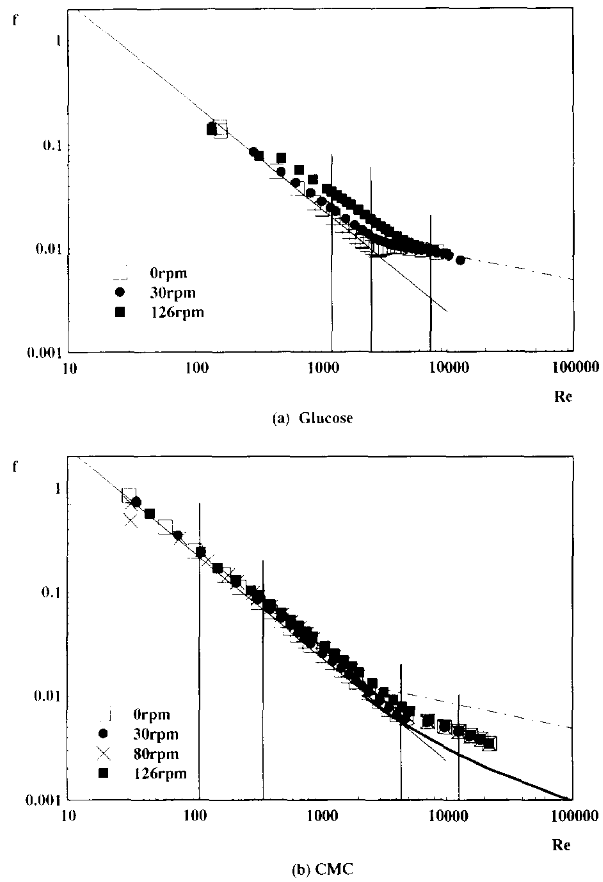

Figure 3 Friction factor *versus* Reynolds number for (a) glucose (b) CMC; ———— · Re = 23.9, —·— Jones and Leung (1981), ———— ultimate drag = reduction asymptote

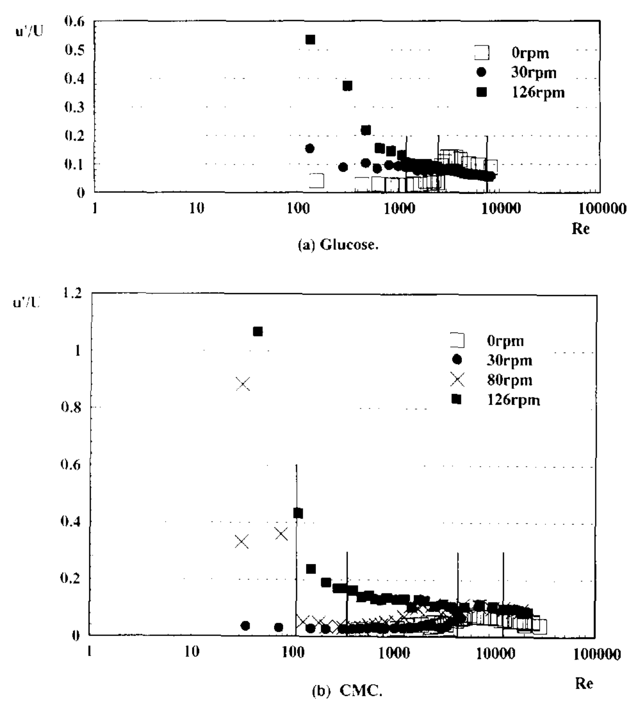

Figure 4 Axial velocity fluctuations at $\xi = 0.8$ for (a) glucose, (b) CMC

The vertical lines in Figures 3 and 4 correspond to the Reynolds numbers at which more detailed data were obtained using the LDA.

Only in the absence of rotation for the glucose–water mixture do the velocity fluctuations show a clear transition from laminar to turbulent flow. The increase in friction factor at the highest rotation speed is also most marked for this fluid. For CMC, the effect of rotation on friction factor is marginal and, in the tubulent-flow regime, it can be seen from Figure 3 that the degree of drag reduction for the polymer is essentially unaffected by rotation. Escudier et al. (1995a) demonstrated the applicability for turbulent annular flow in the absence of centerbody rotation of the scaling proposed by Hoyt (1991) for drag-reducing fluids in pipe flow. Because the influence of rotation on the f–Re curves is negligible, it can be concluded that this scaling is also applicable here. From Figure 4, it is seen that for both fluids there are velocity fluctuations of increasing intensity in the laminar regime as the rotation speed is increased. As discussed later, these fluctuations are associated with the advection of Taylor vortices by the axial flow.

All subsequent figures refer to data for the highest rotation speed (126 rpm) as the bulk Reynolds number is varied. the parameter $U/\omega R_i$ has been chosen to characterize the relative magnitudes of the bulk flow and the rotation speed [i.e., half the inverse of Nouri and Whitelaw's (1994) Rossby number] as well as a Taylor number, defined here as $(\rho\omega/\mu)^2 R_i (R_o - R_i)^3$.

In contrast to the negligible influence on the f–Re data, rotation has a strong influence on the tangential mean velocities (Figure 5), which generally reveal a triple-layer structure. Nouri and Whitelaw (1994) report very similar observations for both a Newtonian fluid and for CMC in the turbulent-flow regime as do Nouar et al. (1987) and Naïmi et al. (1990) for CMC and Carbopol, respectively. Limited measurements showing the triple-layer structure for turbulent airflow were also reported by Simmers and Coney (1979) for a narrow annulus and by Kuzay and Scott (1973) for an annulus with radius ratio 0.56. Perhaps surprisingly, the theoretical work of Bittleston and Hassager (1992) for laminar flow of a Bingham plastic in an annulus also shows the occurrence of such a structure. There is a loose analogy, therefore, between the decrease in effective viscosity in a shear-thinning liquid on the one hand and the decrease from a turbulent to a molecular (Newtonian) viscosity on the other. Taylor (1935) was the first to point out that over much of the central region of the annulus, the mean angular momentum wr for turbulent flow is almost constant. The smooth curves in Figure 5 correspond to distributions of constant angular momentum.

$$wr = C\omega R_i^2$$

with values for the constant C in the range 0.3–0.6. Taylor's measurements, for water flow in an annulus in the absence of an axial flow, gave a value for $C = 0.53$, which is very close to the values found here for all fluids at the lower Reynolds numbers. Taylor pointed out that completely different mechanisms for turbulent transport of momentum and vorticity are required to explain the different distributions of angular momentum that prevail in the central region and the outer layers. Taylor also argued that the mixing length/eddy viscosity concept is incompatible with radial independence of wr, but the argument seems to rest upon a dubious formulation of the mixing-length model for swirling flow. The very abrupt changes in velocity gradient at $\xi \approx 0.1 - 0.2$ and $0.8 - 0.9$ do, indeed, suggest dramatic changes in turbulence structure; although this is not confirmed by the measurements of axial and tangential turbulence intensities. As the Reynolds number is increased, the tangential velocity levels within the annular gap are progressively reduced and, at the highest Reynolds numbers, penetration of the influence of rotation is increasingly confined to an inner layer. This tendency is particularly noticeable for CMC at a Reynolds number of 12,500. The same qualitative behavior was found by Nouri and Whitelaw (1994); the data for Carbopol reported by Naimi et al. (1990) inexplicably exhibited a progressive increase in the tangential velocity level as the Reynolds number was increased. Close to the centerbody, the tangential velocity increases rapidly across a thin layer to match the peripheral speed. As is typical of shear flows generally, this inner-layer thickness decreases with increasing Reynolds number. It is also seen that the inner-layer thickness for the shear-thinning fluid is roughly double that for the glucose–water mixture. Although the outer layer is of comparable overall thickness to the inner layer in each case, it is easily seen that for a Newtonian fluid, the tangential velocity gradients at the inner and outer surfaces are related by the following:

$$\left.\frac{dw}{dr}\right|_i = \omega + \left(\frac{R_o}{R_i}\right)^2 \left.\frac{dw}{dr}\right|_o$$

so that the tangential velocity gradient in the inner layer must be substantially higher than in the outer layer, as the measurements show. This expression is a consequence of the torque being constant within the annular gap and the assumption of laminar sublayers at each surface. The situation for a non-Newtonian fluid is more complex, although, qualitatively, the same trend evidently exists.

The theoretical analysis of Sharma et al. (1976) for turbulent flow of a Newtonian fluid showed that the flow development length increases significantly with increasing values of $U/\omega R_i$.

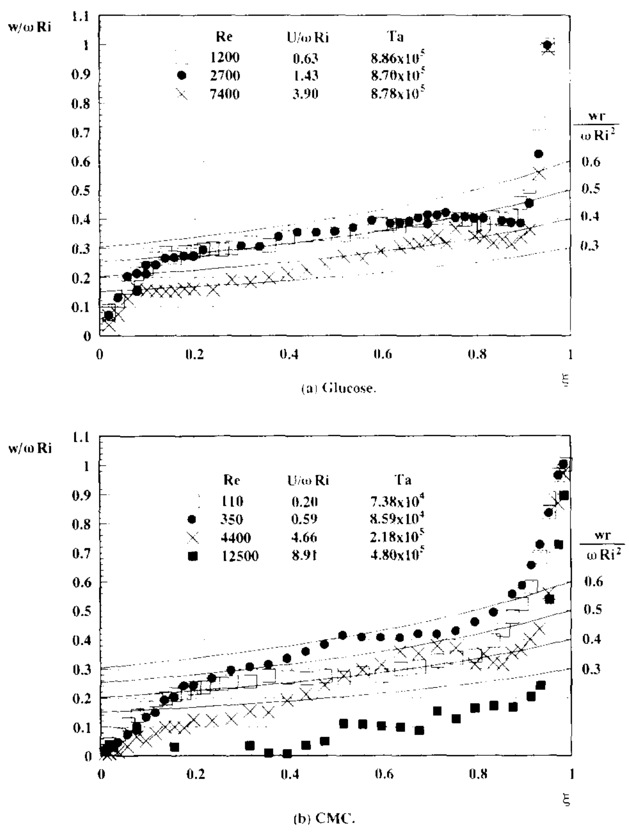

Figure 5 Tangential velocity profiles for (a) glucose, (b) CMC

Their calculations would indicate that, for the present measurements, fully developed conditions were, indeed, reached. The calculations also showed that the value of $C(\equiv wr/\omega R_i^2)$ in the gap center was slightly less than 0.4 but decreased slightly with radius and was essentially independent of Reynolds number and $U/\omega R_i$, although the calculations were limited to Reynolds numbers generally higher than those reached here (17,192–65,898) and, of course, to a Newtonian fluid.

With the exception of the CMC flow at Re = 110, the axial velocity distributions (Figure 6) are little different from what would be expected in the absence of rotation; i.e., a progressive flattening of the profile with increasing Reynolds number, again consistent with earlier investigations. Sharma et al. (1976) also comment on the weak coupling between the axial and swirling flow under turbulent conditions. The apparently spurious behavior for CMC at the lowest Reynolds number is a consequence of averaging the unsteady axial velocities associated with the interior circulation of Taylor vortices that are transported axially by the bulk flow. Even clearer evidence for the presence of Taylor vortices for the low Reynolds number CMC flow is seen in the axial velocity fluctuations (Figure 7b): the two peaks close to $\xi = 0.2$ and 0.8 represent the time-averaged effect of the internal recirculating motion of the Taylor vortices as they are transported axially. In all other cases, the axial velocity fluctuations show a progressive decrease with increasing Reynolds number. This, too, is ascribed to the complex but well-defined structures that are generated by the centerbody rotation at the lower Reynolds numbers.

It is well established (e.g., Pinho and Whitelaw 1990; Escudier et al. 1995a) that for turbulent flow of polymeric fluids in pipe and annular flow, drag reduction is invariably accompanied by suppressed levels of tangential velocity fluctuations. As can be seen from Figure 8, there is some

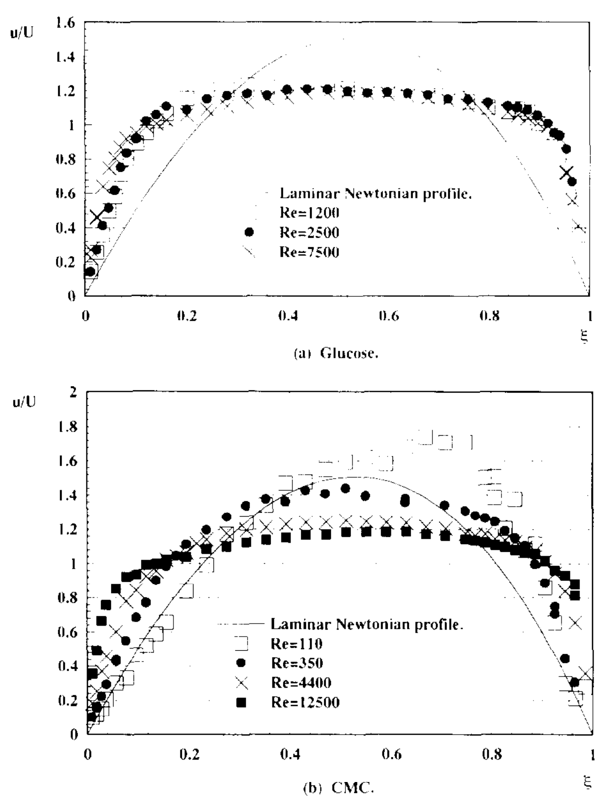

Figure 6 Axial velocity profiles for (a) glucose, (b) CMC

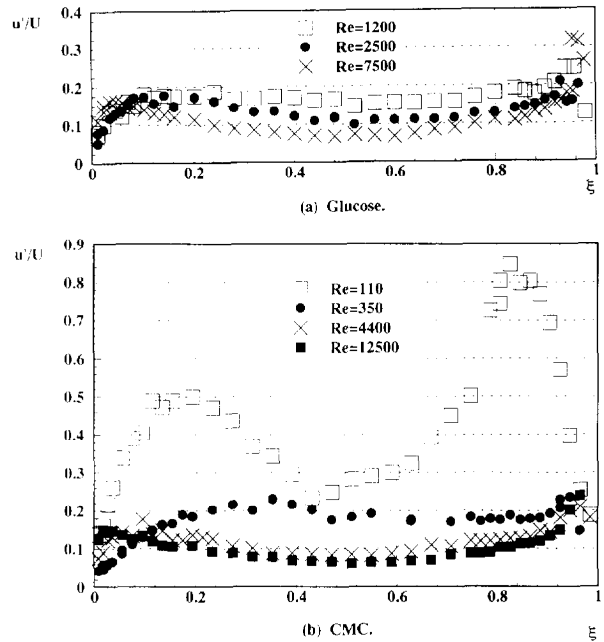

Figure 7 Axial velocity fluctuations for (a) glucose, (b) CMC

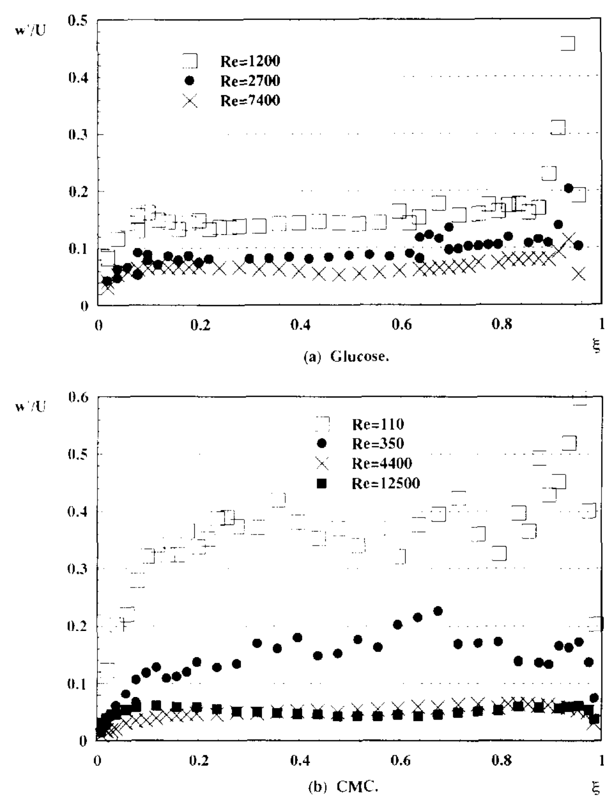

Figure 8 Tangential velocity fluctuations for (a) glucose, (b) CMC

evidence for this behavior here, except for the high fluctuation levels at the lower Reynolds numbers associated with the vortical structures induced by the centerbody rotation. As already seen, at the higher Reynolds numbers the radial penetration of the rotational influence is much reduced, and turbulent fluctuations are again suppressed as if there were no centerbody rotation.

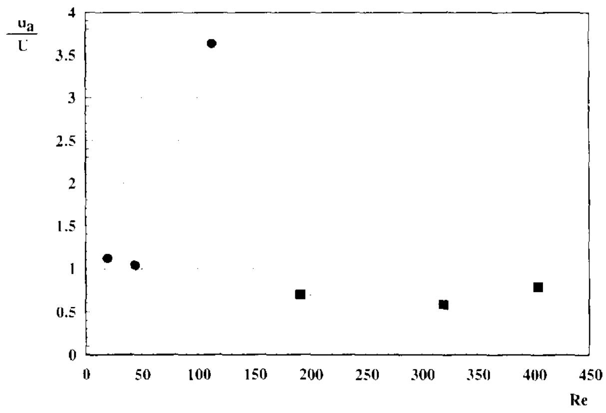

Figure 9 Taylor-cell advection velocities for glucose and CMC; ■, normalized advection velocity (glucose); ●, normalized advection velocity (CMC)

Limited investigations into the structural flow changes at low but increasing bulk velocity were carried out using two identical LDA probes with the probe volumes a set axial distance apart (10 mm or 20 mm) and azimuthally separated by 90°. The velocity–time signals generated by the two probes were cross-correlated to give a time spacing between the flow structure passing each probe and, hence, an advection velocity for the cell structure. Figure 9 shows the change with Reynolds number in the advection velocity normalized with the bulk flow velocity. The normalized advection speed is seen to be about 0.6–0.7 for glucose and to increase from a value of about unity for Re < 50 to values above 2.5 for CMC, suggesting a change from a toroidal to a spiral structure. However, it would require three simultaneous measurements to determine advection speed, cell size, and spinal pitch, and this was not possible with the available instrumentation. A value of unity for the normalized advection speed at the low Reynolds numbers is consistent with the visual estimates of Snyder (1962), which gave an average value for a Newtonian fluid of 1.2 at Reynolds numbers less than 16. For the Newtonian fluid, the signals at higher Reynolds numbers than those shown did not reveal a periodic structure that could be used to determine advection speed.

Conclusions

The influence of centerbody rotation on the pressure drop in concentric annular flow is negligible under turbulent-flow conditions for both a 0.2% aqueous solution of CMC, a shear-thinning polymer, and a Newtonian liquid. Under laminar-flow conditions, there is a modest increase in pressure drop for CMC and a somewhat greater increase for the Newtonian fluid.

The greatest differences in the tangential velocity distributions is in the vicinity of the centerbody and outer wall of the annulus, with considerably higher gradients and thinner "boundary layers" for the Newtonian fluid. Outside these layers, the tangential velocity decreases, roughly speaking, in inverse proportion to the radius. Increasing the bulk velocity (for constant rotational speed) produces a progressive reduction in the level of the tangential velocity that is similar for the two fluids, except for anomalous behavior at low Reynolds number for CMC.

The influence of rotation on the axial velocity distribution is also most apparent at low Reynolds numbers and is attributed to the advection of vortical structures by the bulk motion.

References

Alderman, N. J., Gavignet, A. A., Guillot, D. and Maitland, G. C. 1988. High temperature, high pressure rheology of water-based muds. Society of petroleum Engineers Paper 18035

Bittleston, S. H. and Hassager, O. 1992. Flow of viscoplastic fluids in a rotating concentric annulus. *J. Non-Newstonian Fluid Mech.*, **42**, 19–36

Escudier, M. P., Gouldson, I. W. and Jones, D. M. 1995a. Flow of shear-thinning fluids in a concentric annulus. *Exp. Fluids*. **18**, 225–238

Escudier, M. P., Gouldson, I. W. and Jones, D. M. 1995b. Taylor vortices in Newtonian and shear-thinning liquid. *Proc. R. Soc. A*, **449**, 155–176

Hoyt, J. W. 1991. Negative roughness and polymer drag reduction. *Exp. in Fluids*, **11**, 142–146

Jones, O. C. and Leung, J. M. C. 1981. An improvement in the calculation of turbulent friction in smooth concentric annuli. *J. Fluids Eng.*, **103**, 615–623

Kuzay, T. M. and Scott, C. J. 1973. Turbulent heat and momentum transfer studies in an annulus with rotating inner cylinder. University of Minnesota, Heat Transfer Laboratory, TR No. 111.

Lockett, T. J. 1992. Numerical simulation of inelastic non- Newtonian fluid flows in annuli. Ph.D. thesis, Imperial College of Science, Technology, and Medicine. London, UK

Lockett, T. J., Richardson, S. M. and Worraker, W. J. 1992. The stability of inelastic non-Newtonian fluids in Couette flow between concentric cylinders: A finite-element study. *J. Non-Newtonian Fluid Mech.*, **43**, 165–177

Malik, R. and Shenoy, U. V. 1991. Generalized annular Couette flow of a power-law fluid. *Ind. Eng. Chem. Res.*, **30**, 1950–1954

Naimi, M., Deviene, R. and Lebouche, M. 1990. Étude Dynamique et thermique de l'écoulement de Couette-Taylor-Poiseulle; cas d'un fluide presentant un seuil d'écoulement. *Int. J. Heat Mass Transfer*, **33**, 381–391

Nouar, C., Deviene, R. and Lebouche, M. 1987. Convection thermique pour l'écoulement de Couette avec debit axial; cas d'un fluide pseudo-plastique. *Int. J. Heat Mass Transfer*, **30**, 639–647

Nouri, J. M. and Whitelaw, J. H. 1994. Flow of Newtonian and non-Newtonian fluids in a concentric annulus with rotation of the inner cylinder. *J. Fluids Eng.*, **116**, 821–827

Pinho, F. T. and Whitelaw, J. H. 1990. Flow of non-Newtonian fluids in a pipe. *J. Non-Newtonian Fluid Mech.*, **34**, 129–144

Sharma, B. I., Launder, B. E. and Scott, C. J. 1976. Computation of annular, turbulent flow with rotating core tube. *J. Fluids Eng.*, Dec. 753–758

Simmers, D. A. and Coney, J. E. R. 1979. The experimental determination of velocity distribution in annular flow. *Int. J. Heat Fluid Flow*, **1**, 177–184

Snyder, H. A. 1962. Experiments on the stability of spiral flow at low axial Reynolds numbers. *Proc. R. Soc. A.*, **265**, 198–214

Taylor, G. I. 1935. Distribution of velocity and temperature between concentric rotating cylinders. *Proc. Roy. Soc. A.*, 494–512

Wroński, S. and Jastrzębski, M. 1990a. Experimental investigations of the stability limit of the helical flow of pseudoplastic liquids. *Rheologica Acta*, **29**, 453–461

Wroński, S. and Jastrzębski, M. 1990b. Mass transfer in the spiral flow of a pseudoplastic liquid. *Int. J. Heat Mass Transfer*, **33**, 1–7